Applied Catalysis B: Environmental 125 (2012) 282–287

Contents lists available at SciVerse ScienceDirect

Applied Catalysis B: Environmental

journal homepage: www.elsevier.com/locate/apcatb

Efficient photocatalytic reduction of aqueous Cr(VI) over $CaSb_2O_5(OH)_2$ nanocrystals under UV light illumination

Guodong Chen [b], Meng Sun [a,*], Qin Wei [b], Zhenmin Ma [a,*], Bin Du [a]

[a] School of Resources and Environment, University of Jinan, Jinan 250022, PR China
[b] Key Laboratory of Chemical Sensing & Analysis in Universities of Shandong, School of Chemistry and Chemical Engineering, University of Jinan, Jinan 250022, PR China

ARTICLE INFO

Article history:
Received 10 March 2012
Received in revised form 28 May 2012
Accepted 3 June 2012
Available online 9 June 2012

Keywords:
Photocatalysis
Reduction
Cr(VI)
Ultraviolet
$CaSb_2O_5(OH)_2$

ABSTRACT

$CaSb_2O_5(OH)_2$ nanocrystals were synthesized via traditional and microwave-assisted hydrothermal methods from aqueous solution of $CaCl_2$ and $KSb(OH)_6$, respectively. The structures, Brunauer–Emmett–Teller (BET) specific surface areas and optical properties of the as-synthesized samples were characterized by X-ray diffraction, transmission electron microscopy, N_2 sorption–desorption isotherms, and UV–vis diffuse reflectance spectra. The results of photocatalytic reduction of aqueous Cr(VI) revealed that $CaSb_2O_5(OH)_2$ possessed a superior activity greatly larger than that of commercial P25 (Degussa Co.). It was shown that proton supply played a crucial role in the reduction reaction. The Cr(VI) photo-reduction rates were systematically accelerated as the proton concentration increased in the aqueous suspensions. Formate ions were also shown to exert a dramatic accelerating influence on Cr(VI) reduction in the system. This observation should be rationalized by considering that these species act as hole scavengers in the reduction process. The consequent improvement in quantum yield combines with the protons provided by H_2SO_4 result in the observed rate enhancement.

1. Introduction

The improper discharge of various industrial wastewaters containing toxic wastes has greatly polluted the environment, and this stimulates vigorous investigations about the fundamental and applied research in the environmental remediation [1–4]. The presence of heavy metals in industrial wastewaters has already been known to cause serious pollution problems [5–7]. Cr(VI) is a frequent contaminant in the wastewaters arising from industrial processes, and it is highly mobile in aquatic system due to its solubility. It is toxic to most organisms, and has been classified as carcinogenic and mutagenic its concentration has been strictly regulated [8–12]. Due to its high toxicity and high mobility in water, Cr(VI) has been included in the list of priority pollutants and its concentration in drinking water has been regulated by many countries. The common methods currently adopted to remove heavy metal ions from wastewater including precipitation, adsorption, ion exchange, and membrane separation [1,2]. Each method has its own advantages and disadvantages, and the main factors that influence the efficiencies of these methods are the source of the wastewater and the concentration of the contaminant [13]. While Cr(III) is considered nontoxic in most forms but an essential trace metal in human nutrition, Cr(VI) is usually reduced to Cr(III) in order to minimize environmental pollution [11]. And thus, reactions that reduce Cr(VI) in contaminated waters have received considerable attention because it diminishes or eliminates the threat to aquatic life and to human health posed by Cr(VI) contaminations. However, in the traditional treatment of chromium-bearing wastewaters, in order to convert the hexavalent chromium to the trivalent state reducing agents such as $FeSO_4$, SO_2 or $NaHSO_3$ must be added, which would cause secondary pollution. Development of innovative treatment technologies to remove heavy metals from waste waters is greatly needed.

Reduction by semiconductor photocatalysis technology is a relatively new technique for the removal or recovery of dissolved metal ions in wastewater. For instance, when TiO_2 were illuminated with UV light, highly reductive electrons would be generated and initiate the reduction of heavy metal ions in wastewater. Many researchers have reported the photocatalytic reduction of Cr(VI) over TiO_2 [1,11,14,15]. Yu et al. [16] reported the reduction of Cr(VI) over a TiO_2-boron doped diamond heterojunction. Shaham-Waldmann and Paz [17] reported the photocatalytic reduction of Cr(VI) by titanium dioxide coupled to functionalized carbon nanotubes. However, all of those researches were based on TiO_2 photocatalysis, and the results exhibited that the activity of TiO_2 is very low and the reduction process usually needs a long time. Recently, Zhang et al. [18] reported the photocatalytic reduction of aqueous Cr(VI) over SnS_2 nanocrystals under visible light

* Corresponding authors. Tel.: +86 531 82769235; fax: +86 531 82765969.
E-mail addresses: smlcu@eyou.com (M. Sun), mzmstu@163.com (Z. Ma).

0926-3373/$ – see front matter © 2012 Elsevier B.V. All rights reserved.
http://dx.doi.org/10.1016/j.apcatb.2012.06.001

irradiation, but the activity was still very low. On the other hand, sulfide was commonly not stable enough to be used as photocatalyst. And so, to explore non-TiO_2 based catalyst with high photocatalytic reduce ability is greatly needed.

Previously, we have reported $CaSb_2O_5(OH)_2$ nanocrystals (NCs) as efficient photocatalyst in decomposing aromatic compounds in gas phase and dyes in water [19,20]. With a band gap (4.6 eV) larger than that of TiO_2 (3.2 eV), the photo-generated electrons on the conduction band minimum of $CaSb_2O_5(OH)_2$ NCs would exhibit a stronger reduce ability compared with TiO_2. Herein, we first report the photocatalytic reduction of aqueous Cr(VI) over $CaSb_2O_5(OH)_2$ NCs synthesized with different hydrothermal methods. The results demonstrated that the $CaSb_2O_5(OH)_2$ NCs had strong photocatalytic reduce ability toward aqueous Cr(VI), which was greatly larger than that of commercial P25. The results also revealed that the reduction of aqueous Cr(VI) over $CaSb_2O_5(OH)_2$ NCs was greatly influenced by the addition of sulfuric acid and sacrificial electron donors such as formic acid.

2. Experimental

2.1. Synthesis of $CaSb_2O_5(OH)_2$ nanocrystals

All the reagents are analytical-grade and purchased from Sinopharm Chemical Reagent Co., Ltd. $CaSb_2O_5(OH)_2$ nanocrystals were synthesized by traditional and microwave-assisted hydrothermal method, respectively. In a typical procedure, 25 mL of 0.1 M $CaCl_2$ solution was slowly dropped into 50 mL of $KSb(OH)_6$ (0.1 M) solution under continuous stirring. After 20 min of stirring, the mixture was loaded into a 100 mL Teflon-lined autoclave and maintained at 180 °C for 24 h. After reaction, the product was collected, washed with distilled water, and finally dried in air at 60 °C, the product was labeled as $CaSb_2O_5(OH)_2$—CH. For the microwave hydrothermal synthesis, 25 mL of the resultant mixture was loaded into a 35 mL vessel (20–25 mL reaction volume), which was microwave treated at 180 °C for 20 min using a single mode CEM Discover System (Explorer48, CEM Co., and U.S.A.) operating at 200 W, 2.45 GHz. After reaction, the resulting product was collected, washed, and finally dried in air at 60 °C, the final product was labeled as $CaSb_2O_5(OH)_2$—MH. All of the hydrothermal treatment was made in the absence of dispersant or capping organic agent, avoiding the pollution of environment.

2.2. Characterization of photocatalysts

X-ray diffraction (XRD) patterns were collected on a Bruker D8 Advance X-ray diffractometer at 40 kV and 40 mA with Ni-filtered Cu Kα radiation. Transmission electron microscopy (TEM) and high-resolution transmission electron microscopy (HRTEM) images were taken on a JEOL model JEM 2010 EX instrument at an accelerating voltage of 200 kV. Carbon-coated copper grid was used as the sample holder. UV–vis diffuse reflectance spectroscopy (DRS) were recorded on a UV–vis spectrophotometer (Cary 500 Scan Spectrophotometers, Varian, and U.S.A.) equipped with an integrating sphere attachment. Nitrogen sorption experiment was carried out at 77 K by using Micromeritics ASAP2020 equipment. X-ray photoelectron spectroscopy (XPS) analysis was conducted on an ESCALAB 250 photoelectron spectroscopy (Thermo Fisher Scientific) at 3.0×10^{-10} mbar using Al Kα X-ray beam (1486.6 eV).

2.3. Photocatalytic tests

The photocatalytic experiments were carried out in a home-made quartz tube with 4.6 cm inner diameter and 17 cm length. Four 4 W UV lamps with a wavelength centered at 254 nm (Philips, TUV 4W/G4 T5) were used as illuminating source. The reaction suspension was prepared by adding 0.08 g of the catalyst to 150 mL of 50 mg/L $K_2Cr_2O_7$ aqueous solution, and then a certain amount of 1.0 M H_2SO_4 solution was added to keep an acidic medium. Prior to illumination, the suspension was magnetically stirred in the dark for 1 h to establish an adsorption/desorption equilibrium condition. The aqueous suspension containing Cr(VI) and photocatalyst was then irradiated by UV light with constant stirring. During illumination, about 3 mL of suspension was taken from the reactor at a scheduled interval, which was immediately centrifuged to remove the photocatalyst and complexed to facilitate determining their Cr(VI) concentration. The Cr(VI) content in the 10-fold dilution of the supernatant solution was colorimetrically determined at 540 nm using the diphenylcarbazide (DPC) method with a detection limit of 0.005 mg/L [21]. A blank experiment was carried out using dichromate solution without a photocatalyst in order to determine the extent of reduction of the concentration of hexavalent chromium due to the UV radiation. As a comparison, the photocatalytic reduction of Cr(VI) over P25 was also tested under the same conditions with an equal amount of catalyst added. The percentage of reduction is reported as A_t/A_0. A_t is the absorbance intensity of Cr(VI)–DPC complex at each irradiated time interval of the main peak located at 540 nm. And A_0 is the absorbance intensity of Cr(VI)–DPC complex of the initial concentration when adsorption–desorption equilibrium was achieved.

3. Results and discussion

3.1. Structural characterization

The XRD patterns of the as synthesized $CaSb_2O_5(OH)_2$ NCs are shown in Fig. 1. The relatively wide diffraction peaks of the two samples synthesized with different hydrothermal methods may suggest the small particle sizes. Using the well-known Scherrer formula based on the half-widths of (2 2 2) peak in their XRD patterns, the crystal sizes were calculated and it was found to be 10 nm or so. All the products displayed only the characteristic XRD peaks of pure phase $CaSb_2O_5(OH)_2$ (JCPDS no. 32-0154, bottom of Fig. 1). There is no trace of any impurity phase under the instrument's resolution.

The morphologies of $CaSb_2O_5(OH)_2$ NCs synthesized with traditional and microwave-assisted hydrothermal method are demonstrated in the TEM images shown in Fig. 2. It reveals that the as-synthesized $CaSb_2O_5(OH)_2$ NCs have possessed a diameter of 10 nm. The clear lattice fringes with interlayer spacing of 0.30 and 0.31 nm correspond to the (2 2 2) and (3 1 1) planes of $CaSb_2O_5(OH)_2$, respectively.

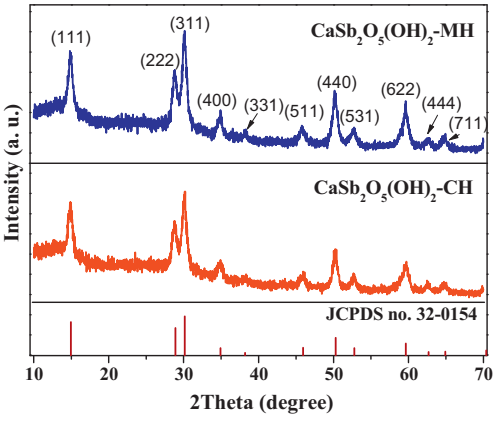

Fig. 1. X-ray diffraction patterns of $CaSb_2O_5(OH)_2$ NCs synthesized with different methods.

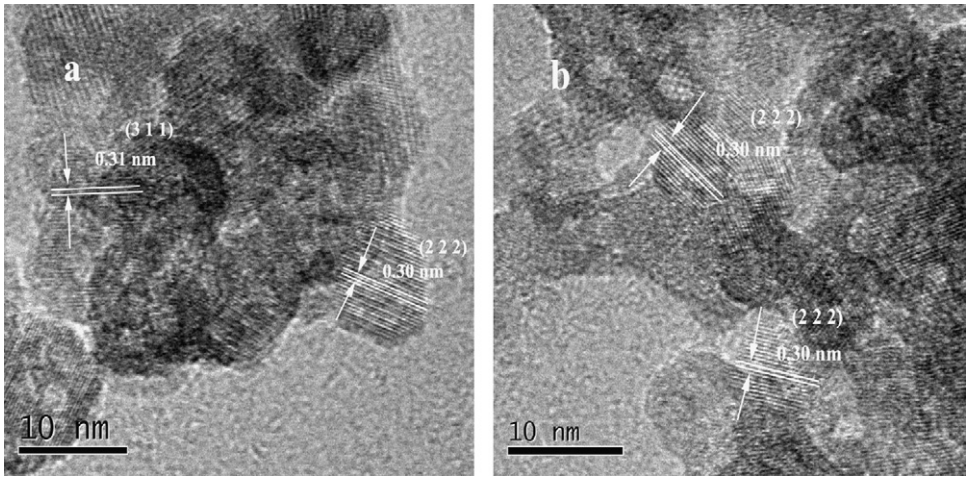

Fig. 2. TEM images of $CaSb_2O_5(OH)_2$ NCs: (a) synthesized by C-H method, (b) synthesized by M-H method.

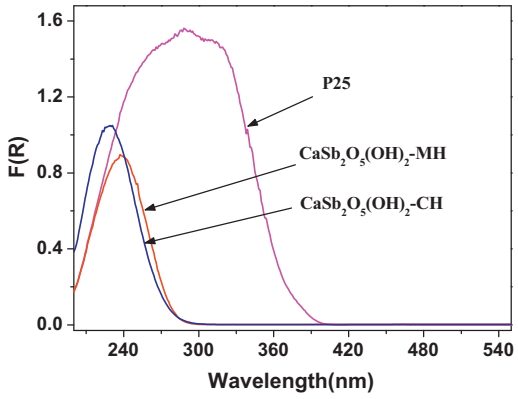

Fig. 3. UV–vis diffuse reflectance spectrum of $CaSb_2O_5(OH)_2$ NCs with P25 as a reference.

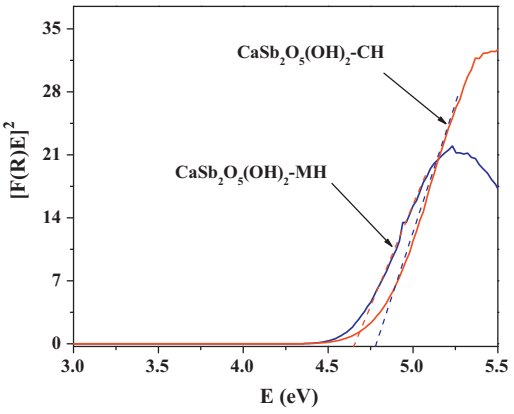

Fig. 4. Optical band gap energy E_g of $CaSb_2O_5(OH)_2$ NCs.

3.2. Optical characterization

The UV–vis diffuse reflectance spectra of $CaSb_2O_5(OH)_2$ NCs were measured and converted into the absorption spectra (shown in Fig. 3) using the Kubelka–Munk function. It was found that the light absorption abilities of the two samples were different. The sample synthesized with traditional hydrothermal method was slightly stronger, and its light absorption edge was also blue shifted. According to the previous study, the relation between absorption coefficient and band-gap energy for direct-gap semiconductor can be described by the formula: $[F(R)E]^2 = A(E - E_g)$, where E, E_g are photon energy and optical band-gap energy, respectively, and A is the characteristic constant of semiconductor. In the equation, $[F(R)E]^2$ has a linear relation with E. Extrapolating the linear relation to $[F(R)E]^2 = 0$ gives the band gap E_g of the sample. As shown in Fig. 4, the band gap of $CaSb_2O_5(OH)_2$ NCs synthesized with traditional hydrothermal (C-H) method is approximately 4.77 eV, while that for the sample synthesized with microwave-assisted hydrothermal (M-H) method was about 4.64 eV.

The results of N_2 sorption–desorption analysis reveals that he BET specific surface area of $CaSb_2O_5(OH)_2$—MH is about 101.8 $m^2\,g^{-1}$, while that of $CaSb_2O_5(OH)_2$—CH was 86.9 $m^2\,g^{-1}$, both of which were larger than that of P25 (50 $m^2\,g^{-1}$).

3.3. Photocatalytic reduction of Cr(VI)

A previous study reported that the reduction rate of aqueous Cr(VI) over photocatalyst was greatly influenced by the pH values in the solutions [1]. To investigate the influences of H_2SO_4 on the photocatalytic reduction of Cr(VI) over $CaSb_2O_5(OH)_2$ NCs, controlled experiments were first carried out with different amounts of H_2SO_4 solution (1 M) added. First, we have studied the photocatalytic reduce activity of $CaSb_2O_5(OH)_2$ NCs synthesized by M-H method. As mentioned in Section 2, the photocatalytic processes were evaluated by monitoring the decolorization of the UV–vis absorption spectra of DPC–Cr(VI) complex solutions. Fig. 5 presents the typical temporal evolution of the spectral changes of DPC–Cr(VI)

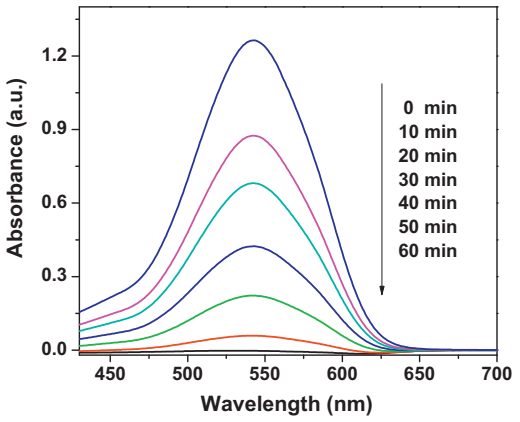

Fig. 5. Time-dependent absorption spectral pattern of DPC–Cr(VI) complex solutions after reduction over $CaSb_2O_5(OH)_2$—MH.

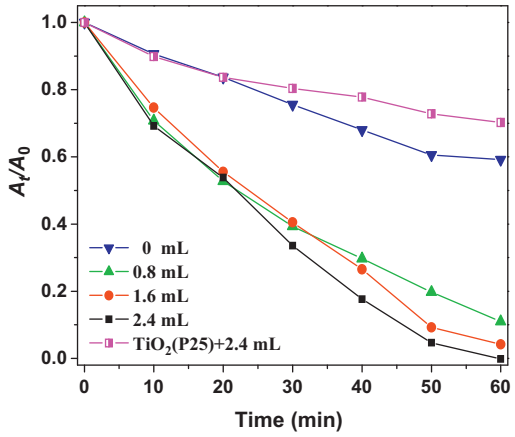

Fig. 6. Photocatalytic reduction of aqueous Cr(VI) over $CaSb_2O_5(OH)_2$–MH under UV irradiation with different amounts of H_2SO_4 solution (1.0 M) added with TiO_2(P25) as a reference.

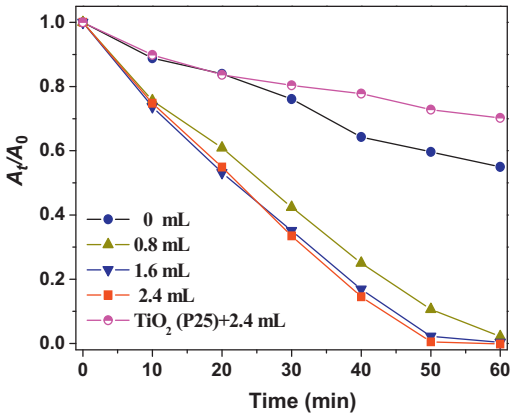

Fig. 8. Photocatalytic reduction of aqueous Cr(VI) over $CaSb_2O_5(OH)_2$—CH under UV irradiation with different amounts of H_2SO_4 solution (1.0 M) added with TiO_2(P25) as a reference.

complex solutions prepared from samples withdrawn from the reactor at various exposure times in the presence of $CaSb_2O_5(OH)_2$—MH. With the increase of irradiation time, the absorption peak located at 540 nm ascribed to DPC–Cr(VI) complex decreased gradually, and after 60 min of irradiation, it almost disappeared.

The temporal concentration variation of Cr(VI) by $CaSb_2O_5(OH)_2$ NCs photocatalytic reduction when different amounts of 1.0 M H_2SO_4 added is shown in Fig. 6. It showed that a addition of H_2SO_4 into the suspension greatly changed the reduction rates of Cr(VI). With the absence of H_2SO_4 the reduction rate was very slow, and after 60 min of continuous reaction the reduction ratio of Cr(VI) was about 40%; when 0.8 mL of 1.0 M H_2SO_4 was added, the reduction ratio was rapidly increased to 89%. Moreover, when 1.6 mL of H_2SO_4 was added, the reduction ratio was 96%, when the amount of H_2SO_4 added was 2.4 mL, the reduction ratio of Cr(VI) was even up to 100%.

For the $CaSb_2O_5(OH)_2$ NCs synthesized by C-H method, we have also tested their photocatalytic reduction toward Cr(VI) under the same conditions, and very similar phenomenon has been observed. Fig. 7 presents the visible spectral changes of DPC–Cr(VI) complex solutions at various exposure times in the presence of $CaSb_2O_5(OH)_2$—CH. After only 50 min of irradiation, the absorption peak located at 540 nm ascribed to DPC–Cr(VI) complex almost disappeared. Thus, the Cr(VI) reduction rate over $CaSb_2O_5(OH)_2$—CH was slightly higher than that over $CaSb_2O_5(OH)_2$—MH. The temporal concentration variation of Cr(VI) in the photocatalytic reduction process under different acidity levels is shown in Fig. 8. It also exhibited that the amount of H_2SO_4 added influenced the reduction rates of Cr(VI) more severely. Without the addition of H_2SO_4 the reduction rate is very low, but when 0.8 mL of 1.0 M H_2SO_4 was added, the reduction ratio after 60 min reaction was rapidly increased to 97%. However, when the H_2SO_4 solution added was more than 1.6 mL, the reduction rate of Cr(VI) in aqueous solutions would keep unchanged.

Fig. 9 shows the photocatalytic reduction of aqueous Cr(VI) in the absence/presence of photocatalyst with 2.4 mL of H_2SO_4 solution added. As can be seen from Fig. 9, in the absence of any photocatalyst, the reduction of Cr(VI) hardly occurred under UV irradiation for 50 min. In the presence of TiO_2 (P25), after 50 min of continuous reaction the reduction ratio of Cr(VI) was about 27%. Instead, the reduction of Cr(VI) proceeded quite rapidly in the presence of $CaSb_2O_5(OH)_2$ NCs synthesized by M-H or C-H method. And thus, $CaSb_2O_5(OH)_2$ NCs exhibited superior reduction ability stronger than that of the widely used P25 photocatalyst.

Except for the addition of acid, another way to promote the photocatalytic performance of the reaction system is to add sacrificial electron donors (hole scavenger). Different kinds of sacrificial reagents are commonly found to have different effects in various systems. Accordingly, choosing a suitable and effective sacrificial reagent is especially important for the improvement of the catalytic performance. In this study, formic acid with its simple one-carbon

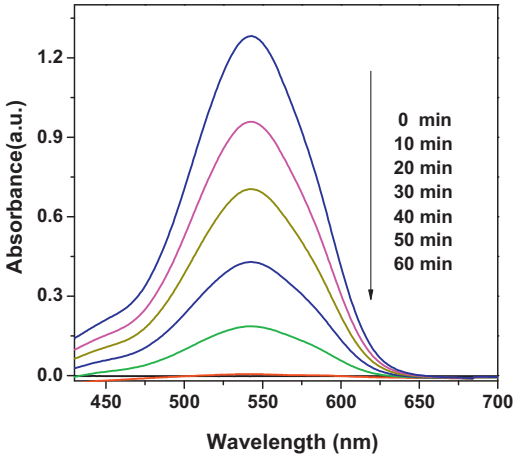

Fig. 7. Time-dependent absorption spectral pattern of DPC–Cr(VI) complex solutions after reduction over $CaSb_2O_5(OH)_2$—CH.

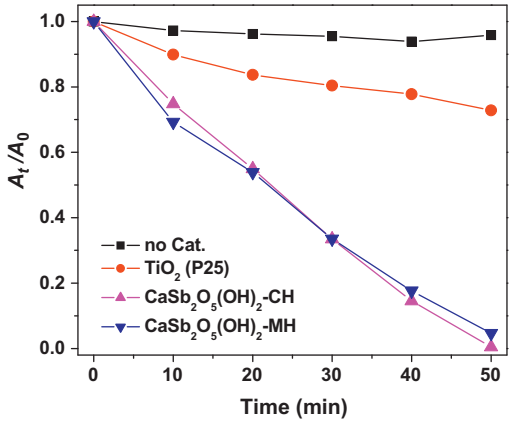

Fig. 9. Photocatalytic activities of $CaSb_2O_5(OH)_2$ NCs and P25 in the reduction of aqueous Cr(VI) under the same reaction conditions.

molecular structure was chosen as a hole scavenger and its effect on Cr(VI) reduction was investigated. Its oxidation to carbon dioxide is straightforward and involves minimal intermediate products [22,23]. Also, formic acid is capable of forming reducing radicals, which can help in the reduction reaction [24]. In the presence of formic acid, the Cr(VI) reduction reaction can be expressed as follows:

$$Cr_2O_7^{2-} + 14H^+ + 6e^- \rightarrow 2Cr^{3+} + 7H_2O \quad (1)$$

In this reaction, for 1 mol of Cr(VI) being reduced to Cr(III) would consume 6 mol of electron, that is to say an equivalent of 6 mol of HCOOH was needed to scavenge the holes. This mechanism is in good agreement with the previously reported experiments [25]. Organic species such as HCOOH accept holes from the valence band bottom either directly or indirectly and are subsequently oxidized, thereby suppressing the electron–hole recombination process and increasing the reduction efficiency. Thus, formic acid can reduce Cr(VI) to Cr(III). Our experiments confirmed that using hole scavenger such as formic acid could greatly accelerate the photocatalytic reduction of Cr(VI). Fig. 10 shows the UV light photocatalytic reduction of aqueous Cr(VI) in the absence/presence of formic acid with 2.4 mL of 1 M H_2SO_4 solution added. In the front part we discussed the influences of H_2SO_4 on the photocatalytic reduction of Cr(VI), and found that when the amount of H_2SO_4 solution added was more than 1.6 mL, the reduction rate of Cr(VI) would no longer be affected by the increase of acidity. Thus, the changes of reduction rate of Cr(VI) must be ascribed to the added hole scavenger ($HCOO^-$). As we can see in Fig. 10, the reduction rates of Cr(VI) have been greatly accelerated when increasing the amount of formic acid added. With the absence of formic acid, the reduction ratio of Cr(VI) in the first 10 min of reaction was only 25%, while in the presence of formic acid with initial concentrations of 14, 47, or 95 ppmv with other conditions unchanged, the reduction ratio was respectively increased to 40%, 46%, and 67%.

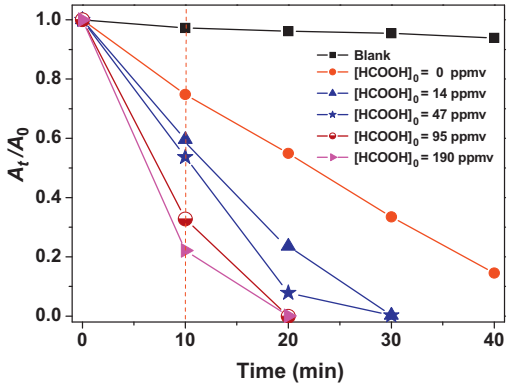

Fig. 10. Kinetics of photocatalytic reduction of aqueous Cr(VI) by $CaSb_2O_5(OH)_2$—CH under UV light by HCOOH as hole scavenger.

When the concentration of formic acid increased to 190 ppmv, the Cr(VI) reduction ratio had been improved to 78%, more than three times larger than that without addition of formic acid. The consumption of formic acid was in proportion to the enhancement of photocatalytic reduction of Cr(VI). The addition of formic acid used as a sacrificial agent efficiently depleted the photo-generated holes and significantly increased the photocatalytic reduction of Cr(VI).

3.4. XPS analysis

Since the stability of a photocatalyst is important for its practical application, the as-synthesized $CaSb_2O_5(OH)_2$ NCs collected after the photocatalytic reduction of aqueous Cr(VI) were further characterized by means of XRD and XPS. Fig. 11 showed the XPS spectra for $CaSb_2O_5(OH)_2$—CH before and after photocatalytic reduction. The survey XPS spectra of samples before and after reaction were almost the same. The high resolution XPS spectra showed that the

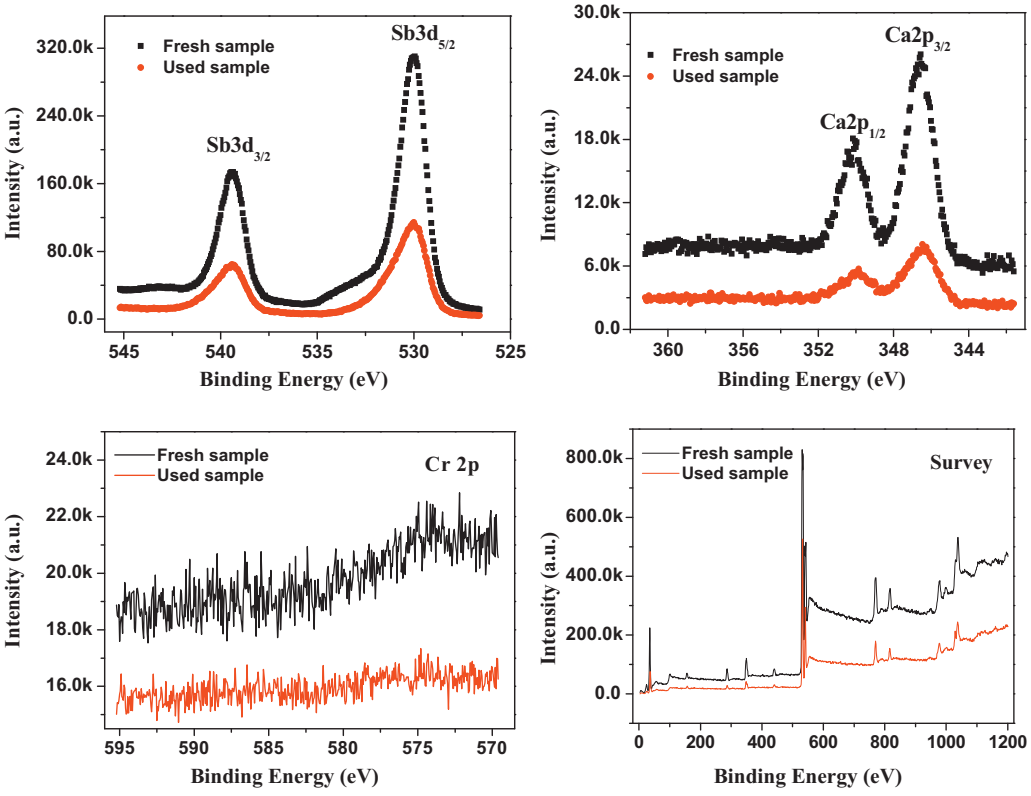

Fig. 11. XPS spectra of $CaSb_2O_5(OH)_2$—CH before and after photocatalytic reduction.

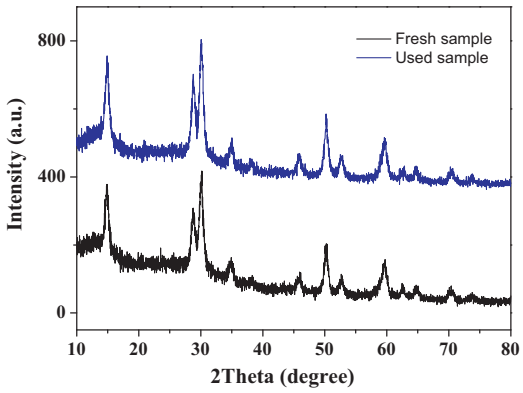

Fig. 12. XRD patterns of $CaSb_2O_5(OH)_2$—CH before and after photocatalytic reduction.

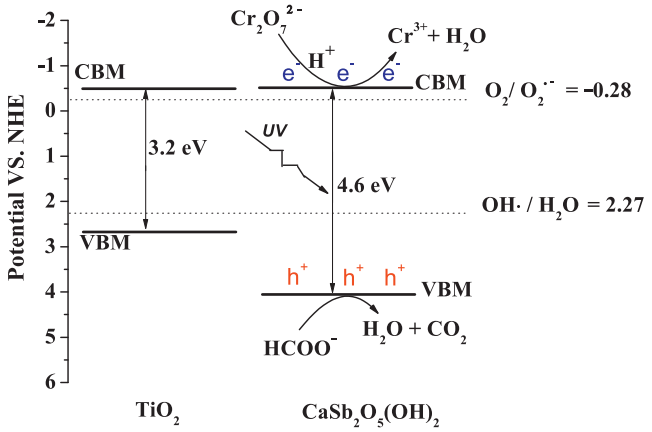

Scheme 1. Proposed mechanism of the photocatalytic reduction of aqueous Cr(VI) over $CaSb_2O_5(OH)_2$ NCs.

binding energies for Ca2p and Sb3d of the fresh sample were nearly the same as that of the used sample, indicating the good chemical stability of the sample in the reaction process. Interestingly, in the narrow scan spectra of the Cr2p no peaks have been observed, suggesting that Cr(III) cations could hardly be absorbed on the surface of catalyst but dissolved in the solution. The following XRD patterns (shown in Fig. 12) of the used sample have shown no obvious change compared to that of the fresh, indicating the stability of $CaSb_2O_5(OH)_2$ NCs.

In rationalizing these results, we have to consider the factors that influenced the overall photocatalytic activities of catalysts, such as the adsorption ability toward reactants, separation ratio of photo-generated electron/hole pairs and their transporting rate, and last the band gap energy [26]. First, the $CaSb_2O_5(OH)_2$ NCs synthesized by M-H and C-H method respectively possessed a band gap of 4.64 and 4.7 eV, both of which were larger than that of P25 (3.2 eV). This larger band gap endows the photo-generated holes and electrons over $CaSb_2O_5(OH)_2$ NCs with strong redox ability. Second, the surface area of $CaSb_2O_5(OH)_2$—MH and $CaSb_2O_5(OH)_2$—CH was respectively 101.8 and 86.9 $m^2\ g^{-1}$, both of which were greatly larger than that of P25(50 $m^2\ g^{-1}$). The larger surface area should be favorable for the adsorption of Cr(VI) over the surfaces of photocatalysts. For the strong absorption of reactant on the surface, it becomes easier for Cr(VI) to react with the photo-generated electrons on the catalyst surface. This was a very important reason to explain why the activity of $CaSb_2O_5(OH)_2$ was higher than that of P25. Third, $CaSb_2O_5(OH)_2$ NCs is a *p*-block metal oxyhydroxide, which contains a central metal ion with d^{10} electronic configuration. It has been reported that the d^{10} electronic configuration was favorable for the separation of photo-generated electron/hole pairs because of the highly dispersive conduction band [27]. Based on the discussion above, a possible mechanism for the reduction of aqueous Cr(VI) over $CaSb_2O_5(OH)_2$ was proposed (Scheme 1).

4. Conclusions

In summary, $CaSb_2O_5(OH)_2$ NCs were synthesized via microwave-assisted and traditional hydrothermal methods, both of which possessed superior activities greatly larger than that of P25 in the photocatalytic reduction of aqueous Cr(VI). The reduction rates of Cr(VI) were greatly accelerated because of the supply of proton. Formic acid as hole scavenger had improved the quantum yield and efficiently increased the reduction rate. With the high photocatalytic reduction ability, it probably has potential application in the reduction of other heavy metal ions in water.

Acknowledgments

This work was financially supported by the NSFC of China (21103069 and 40672158), Special Project of National Department of Science and Technology (2009ZX07212-003), and Scientific Research Foundation for Doctors of University of Jinan (XBS1037, XKY1043).

References

[1] Y. Ku, I.L. Jung, Water Research 35 (2001) 135–142.
[2] S. Rengaraj, S. Venkataraj, J.W. Yeon, Y. Kim, X.Z. Li, G.K.H. Pang, Applied Catalysis B: Environmental 77 (2007) 157–165.
[3] J.S. Hu, L.L. Ren, Y.G. Guo, H.P. Liang, A.M. Cao, L.J. Wan, C.L. Bai, Angewandte Chemie International Edition 44 (2005) 1269–1273.
[4] D.Z. Li, Z.X. Chen, Y.L. Chen, W.J. Li, H.J. Huang, Y.H. He, X.Z. Fu, Environmental Science and Technology 42 (2008) 2130–2135.
[5] J. Munoz, X. Domenech, Journal of Applied Electrochemistry 20 (1990) 518–521.
[6] J. Domenech, M. Andres, Gazzetta Chimica Italiana 117 (1987) 495–498.
[7] N.S. Foster, R.D. Noble, C.A. Koval, Environmental Science and Technology 27 (1993) 350–356.
[8] R. Vinu, G. Madras, Environmental Science and Technology 42 (2008) 913–919.
[9] J.J. Testa, M.A. Grela, M.I. Litter, Environmental Science and Technology 38 (2004) 1589–1594.
[10] S. Luo, Y. Xiao, L. Yang, C. Liu, F. Su, Y. Li, Separation and Purification Technology 79 (2011) 85–91.
[11] B. Sun, E.P. Reddy, P.G. Smirniotis, Environmental Science and Technology 39 (2005) 6251–6259.
[12] N. Wang, L. Zhu, K. Deng, Y. She, Y. Yu, H. Tang, Applied Catalysis B: Environmental 95 (2010) 400–407.
[13] L.B. Khalil, W.E. Mourad, M.W. Rophael, Applied Catalysis B: Environmental 17 (1998) 267–273.
[14] L.M. Wang, N. Wang, L.H. Zhu, H.W. Yu, H.Q. Tang, Journal of Hazardous Materials 152 (2008) 93–99.
[15] C.R. Chenthamarakshan, K. Rajeshwar, Langmuir 16 (2000) 2715–2721.
[16] H.B. Yu, S. Chen, X. Quan, H.M. Zhao, Y.B. Zhang, Environmental Science and Technology 42 (2008) 3791–3796.
[17] N. Shaham-Waldmann, Y. Paz, Journal of Physical Chemistry C 114 (2010) 18946–18952.
[18] Y.C. Zhang, J. Li, M. Zhang, D.D. Dionysiou, Environmental Science and Technology 45 (2011) 9324–9331.
[19] M. Sun, D.Z. Li, Y. Zheng, W.J. Zhang, Y. Shao, Y.B. Chen, W.J. Li, X.Z. Fu, Environmental Science and Technology 43 (2009) 7877–7882.
[20] M. Sun, D.Z. Li, Y.B. Chen, W. Chen, W.J. Li, Y.H. He, X.Z. Fu, Journal of Physical Chemistry C 113 (2009) 13825–13831.
[21] A. Idris, N. Hassan, R. Rashid, A.F. Ngomsik, Journal of Hazardous Materials 186 (2011) 629–635.
[22] M.A. Aguado, M.A. Anderson, Solar Energy Materials and Solar Cells 28 (1993) 345–361.
[23] S. Sanuki, T. Kojima, K. Arai, S. Nagaoka, H. Majima, Metallurgical and Materials Transactions B: Process Metallurgy and Materials Processing Science 30 (1999) 15–20.
[24] M. Kaise, H. Nagai, K. Tokuhashi, S. Kondo, S. Nimura, O. Kikuchi, Langmuir 10 (1994) 1345–1347.
[25] T. Papadam, N.P. Xekoukoulotkis, I. Poulios, D. Mantzavinos, Journal of Photochemistry and Photobiology A: Chemistry 186 (2007) 308–315.
[26] W.K. Chang, K.K. Rao, H.C. Kuo, J.F. Cai, M.S. Wong, Applied Catalysis A: General 321 (2007) 1–6.
[27] H. Xue, Z.H. Li, L. Wu, Z.X. Ding, X.X. Wang, X.Z. Fu, Journal of Physical Chemistry C 112 (2008) 5850–5855.